Supporting Information

Control of single-molecule junction conductance of porphyrins via transition metal center

Zhen-Fei Liu[1]*, Sujun Wei[2], Hongsik Yoon[3], Olgun Adak[4], Ingrid Ponce[4], Yivan Jiang[2], Woo-Dong Jang[3], Luis M. Campos[2]*, Latha Venkataraman[4]*, and Jeffrey B. Neaton[1,5,6]*

[1]Molecular Foundry and Materials Sciences Division, Lawrence Berkeley National Laboratory, Berkeley, California 94720, USA

[2]Department of Chemistry, Columbia University, New York, New York 10027, USA

[3]Department of Chemistry, Yonsei University, 50 Yonsei-ro, Seodaemun-gu, Seoul 120-749, Republic of Korea

[4]Department of Applied Physics and Applied Mathematics, Columbia University, New York, New York 10027, USA

[5]Department of Physics, University of California, Berkeley, California 94720, USA

[6]Kavli Energy Nanosciences Institute at Berkeley, Berkeley, California 94720, USA

Corresponding Author

zfliu@lbl.gov and lcampos@columbia.edu and lv2117@columbia.edu and jbneaton@lbl.gov.

Theory

1) Detailed information on optimization of the geometry

Regarding how the gap between the two electrodes is determined, as described in the main text, we use four atomic layers of gold on each side of the junction, but fix the outer two layers on each side as their bulk geometry. The *z* components of these atoms are allowed to relax, where *z* is the transport axis, along the junction and perpendicular to the atomic surface of the leads. For each side, the force on the *z* component of the outer two Au layers is taken as an average of the *z*-component forces on the atoms of the third layer from the outmost layer. As a result, all of the *x*, *y*, and *z* components of the inner four layers (two on each side) of gold, the adatoms and the molecule, and the *z* components of

the outer four layers (two on each side) of gold are allowed to relax. The gap between the two electrodes is thus optimized. 100Å is used as the length of the simulation box along *z* direction, much greater than the distance between the two outmost layers.

With the optimization scheme above, the orientation of the molecular plane with respect to the gold layer is optimized. The initial geometry is constructed based on the following consideration: there are long alkyl chains in the molecules used in experiment (see Figure 1 of the main text), but in the calculation, we replace those chains to $-CH_3$. If we define θ as the angle between the molecular plane and the gold surface, those long alkyl chains will prevent θ from being too low or too high, otherwise the long alkyl chains would be in contact with the innermost gold surface, on one side or on the other. The angle between the molecular plane (inner porphyrin plane containing the metal) and the gold surface is about 55°.

2) Self-energy corrections with hybrid functionals

As detailed in the main text, fully self-consistent DFT-OT-RSH calculations with our junction geometries, which consist of 1019 atoms, are currently prohibitive. However, we can build information from OT-RSH into DFT+Σ, as follows, correcting the T(E) and conductance. In the DFT+Σ method[1], a self-energy correction of the following form is applied to the eigenvalues of the Hamiltonian of the combined system, e.g.,

$$\Sigma = \sum_{i}^{N_m} \Delta_i \left|\psi_i^{mol}\right\rangle\left\langle\psi_i^{mol}\right|,$$

where N_m is dimension of the molecular subblock, and ψ_i^{mol} is an eigenfunction of the subblock. Although in general Σ is orbital dependent, Δ_i can typically be approximated to be Δ_{HOMO} for all occupied orbitals, and Δ_{LUMO} for all virtual orbitals. For each orbital, Δ is defined as the sum of two terms, e.g.,

$$\Delta = \Sigma_{gp} + \Sigma_{img},$$

where the first term Σ_{gp} accounts for the inaccuracy of the DFT gas phase frontier orbital energy, and the second term Σ_{img} accounts for nonlocal surface polarization effects and is approximated by static image charges[2].

Usually, Σ_{gp} is approximated by the difference between the IP (calculated from ΔSCF or GW) and the PBE HOMO energy. However, as shown in the main text, the dominating conducting orbitals are incorrectly ordered for metal-porphyrin junctions; further, for the OT-RSH functional, by construction, the IP is same as HOMO energy. Thus, we may correct these two PBE errors - qualitatively incorrect orbital ordering and quantitatively inaccurate HOMO energies - simultaneously by equating the difference between OT-RSH HOMO and PBE conducting orbital (not necessarily HOMO) with Σ_{gp} for the systems considered in this work. Σ_{img} is calculated using molecular Mulliken charges interacting with their images, with two image planes taken to be 1.47Å above each surface.

We report the self-energy corrections, computed with DFT+Σ as described above, in the Table S1 below for all four junctions. For open-shell systems such as CuP and CoP, we use same correction for both spin components, and the correction is determined by the following consideration: since a ΔSCF calculation with the OT-RSH[3] functional predicts that the spin states of both CuP and CoP cations are triplets, the minority spin electron is removed when forming a cation. We then correct the PBE conducting orbitals of minority spin component (not necessarily the HOMO) using the OT-RSH minority spin HOMO eigenvalue, provided that the inner product of the PBE conducting orbital and OT-RSH HOMO is nearly unity, and apply this correction to both spin components in the junction calculation with PBE.

As mentioned above, for the systems studied in this work, the parameters used in the OT-RSH functional are $\alpha = 0.2$ and $\gamma = 0.1$. α is fixed based on previous work[4,5], and γ is tuned to minimize[3]

$$J = |\varepsilon_{HOMO}(N) + I(N)| + |\varepsilon_{HOMO}(N+1) + I(N+1)|,$$

where $\varepsilon_{HOMO}(N)$ is the HOMO of N−electron neutral system, I(N) is the ionization potential (IP) of N−electron neutral system, etc. We test the functional with the chosen parameters using a similar molecule, PhNiP in Fig. 1 of the main text, whose IP is known

from experiment to be 6.44 eV[6]. Our OT-RSH calculations, using the parameters described above, predict an IP of 6.31 eV, in excellent agreement with experiment.

We note that in this work, the PBE spin splitting remains unaltered by the self-energy correction described above. Relaxing this constraint is a future direction of study. Also for simplicity, we shift all occupied levels by the same amount Δ downwards (see Table S1), and shift all unoccupied levels by the same amount Δ upwards. [For the minority spin component of CoPc, the Δ shift applies to HOMO-2 (PBE conducting orbital) and all occupied levels below. However, PBE's HOMO and HOMO-1 are also weakly coupled, as seen in the dashed blue curve in Fig. S1. PBE's HOMO corresponds to OT-RSH's HOMO-3. Using a similar strategy, we shift HOMO and HOMO-1 by 2.7 eV downwards.] This shift procedure is justified by the fact that T(E) near E_F, in this case, is entirely dominated by one channel (the quasiparticle HOMO, again, not necessarily PBE HOMO for some systems) for all systems considered in this work, and the energies of the other levels do not numerically affect the predicted conductance.

Table S1: Summary of quantities related to self-energy corrections used in our calculations. For open-shell systems such as CuP and CoP, the minority spin eigenvalues are listed in parentheses. ε_{PBE} is the PBE conducting orbital energy, determined by comparing the eigenchannel (calculated using the Inelastica package[7]) and PBE gas phase orbitals of the isolated molecule; $E_F - \varepsilon_{PBE}$ is the PBE alignment between the Fermi level and the PBE conducting orbital energy, determined from the peak in projected density of states (PDOS) of the junction on the molecule; ε_{gas} (PBE) is the gas phase PBE eigenvalue of the corresponding conducting orbital; ε_{gas} (RSH) is the eigenvalue of gas phase OT-RSH HOMO, which is very similar to IP predicted by OT-RSH, by construction[3]; Σ_{gp} is the difference between the OT-RSH HOMO energy and the gas-phase PBE eigenvalues for conducting orbital, and for open-shell molecules such as CuP and CoP, this is calculated from the minority spin component (see discussion in text) and applied to both spin components. It corrects for the inaccuracy of PBE eigenvalues. The image charge correction Σ_{img} is calculated using Mulliken charges interacting with their own images, assuming image planes at 1.47Å above each surface. It accounts for non-local surface polarization effects[2]. $\Delta = \Sigma_{gp} + \Sigma_{img}$ is the total self-energy correction. The sum of $E_F - \varepsilon_{PBE}$ and Δ is the adjusted level alignment, which would be approximately the HOMO peak in PDOS if OT-RSH functional calculation were performed on the entire junction. All values are in eV.

	FP	CuP	CoP	NiP
ε_{PBE}	HOMO	HOMO (HOMO)	HOMO (HOMO-2)	HOMO-3
$E_F - \varepsilon_{PBE}$	0.25	0.25 (0.38)	0.42 (0.41)	0.51
ε_{gas} (PBE)	-4.18	-3.95 (-4.27)	-4.09 (-4.30)	-4.29
ε_{gas} (RSH)	-5.77	-5.86 (-5.85)	-5.89 (-5.89)	-5.88
Σ_{gp}	1.59	1.58	1.59	1.59
Σ_{img}	0.33	0.33	0.33	0.33
Δ	1.26	1.25	1.26	1.26
$E_F - \varepsilon_{PBE} + \Delta$	1.51	1.50 (1.63)	1.68 (1.67)	1.77

3) Landauer formula using DFT+Σ

We apply Σ only to the molecular subblock of the Hamiltonian of the electrode-molecule-electrode junction, leaving everything else at the PBE level in the transport calculation based on Landauer formula[8,9]. This is justified, as self-energy corrections to Au eigenvalues are negligible compared to those of the molecule. We implement DFT+Σ in the NEGF-based TranSIESTA package[10]. The transmission function is calculated as

$$T(E) = Tr\left\{\Gamma_L^{PBE}(E)\mathrm{G}_C^{mod}(E)\Gamma_R^{PBE}(E)\mathrm{G}_C^{mod\dagger}(E)\right\},$$

where Γ_L^{PBE} (Γ_R^{PBE}) describes the coupling between the extended molecule and the left (right) electrode, and is calculated at PBE level. The modified Green's function G_C^{mod} of the central region is calculated as:

$$\mathrm{G}_C^{mod}(E) = [ES - H^{mod} - \Sigma_L^{PBE}(E) - \Sigma_R^{PBE}(E)]^{-1},$$

where S is the overlap matrix, Σ_L^{PBE} (Σ_R^{PBE}) is the self-energy due to left (right) lead Hamiltonian, and $\Gamma_L^{PBE} = i\left(\Sigma_L^{PBE} - \Sigma_L^{PBE\dagger}\right)$. $\mathrm{H}^{\mathrm{mod}}$ is the Hamiltonian of the extended molecule corrected with the model GW approach DFT+Σ, as described in the main text:

$$H^{mod} = H_S^{PBE} + \Sigma_{mol},$$

where H_S^{PBE} is the PBE Kohn-Sham Hamiltonian of the extended molecule and Σ_{mol} is shift to DFT eigenvalues and is not to be confused with the self-energy due to the leads. Our calculations within this modified NEGF formalism is equivalent to previous work based on scattering theory[1,11]. Within the tight-binding-like first-principles scheme implemented in TranSIESTA[10] using a short-ranged atomic-centered basis, the Γ_{L} (Γ_{R}) matrix, whose dimension is same as the left (right) electrode, should be non-zero only in the upper left (lower right) corner. We set all other elements to zero, to eliminate numerical noise for very low transmission values $\mathrm{T(E)} \sim 10^{-5}\mathrm{G}_0$. This procedure does not have any numerical effect for $\mathrm{T(E)} > 10^{-3}\mathrm{G}_0$. We discuss this further in section (5) below.

4) Spin-dependent T(E) for CoP and CuP

For the two open-shell systems (CuP and CoP), conductances for both spin components are similar, as the HOMO resonance of both spin components are far away from Fermi level of the junction, and spin splitting is small. We show spin-dependent transmission function T(E) for CoP and CuP in Figure S1, calculated both from PBE and DFT+Σ.

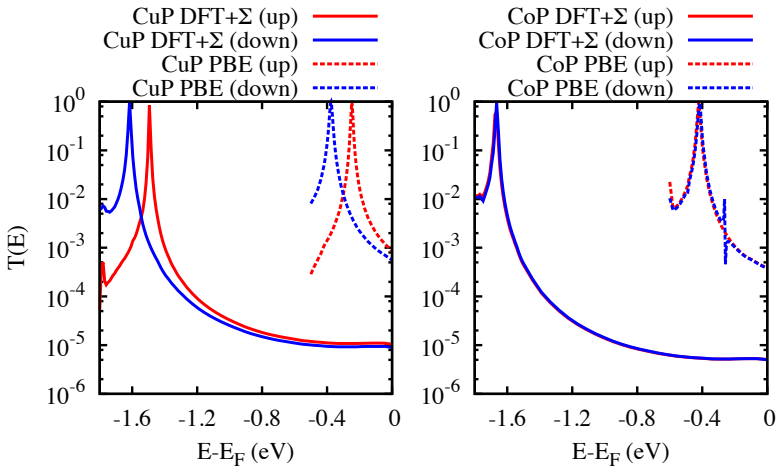

Figure S1: Spin-dependent transmission T(E) for CuP (left panel) and CoP (right panel). Solid lines are DFT+Σ results and dashed lines are DFT-PBE results. DFT+Σ uses OT-RSH functionals (see main text). Red lines are for the up (majority) spin component, and blue lines are for the down (minority) spin component.

5) The block-zero form of coupling matrices

We explain the block-zero form of Γ_L and Γ_R we used in section (3) above. This is used to eliminate numerical noise in T(E) curve, and it is important when T(E) is as low as 10^{-4} (such as the case with the metal porphyrins). We only list the necessary steps relevant towards this purpose. For the complete derivation and implementation of NEGF, we refer the readers to Ref. 10 and Ref. 12.

Figure S2 shows the relaxed CuP junction geometry in our transport calculation, but the discussion is not limited to this particular molecular junction. In our work, each layer contains 8×8 gold atoms. The extended molecule includes the bare molecule and four layers of gold on each side (red boxes). As we explained in the main text, four layers of

gold atoms in the extended molecule are required to converge our results. Within the extended molecule, we denote the left four layers of gold with a lowercase *l*, and the right four layers of gold with a lowercase *r*. We also denote the extended molecule (*l*+mol+*r*) the central region C. There are additional three layers of gold (blue boxes) that are treated explicitly on each side of the extended molecule. They are repeated periodically to -∞ and +∞, respectively, to form the semi-infinite left and right leads. We denote them uppercase L and R. Periodic boundary conditions are used along x and y directions, but not along z which is the direction of current flow.

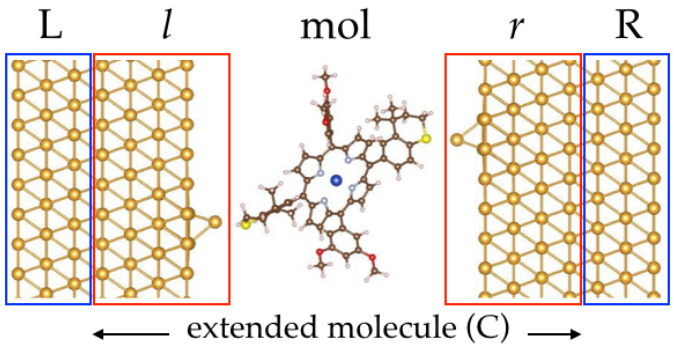

Figure S2: The relaxed CuP junction geometry in our transport calculation. This is used to show the different regions in the junction, and the discussion in this appendix is not limited to these metal-porphyrin junctions. The extended molecule includes the molecule and four layers of gold atoms on each side (red boxes). Three layers of gold atoms (blue boxes) serve as left and right leads. For details, see text.

The Hamiltonian for the system can be written as:

$$\begin{pmatrix} \ddots & -t_L & & & \\ -t_L & H_L & V_L & 0 & \\ & V_L^\dagger & H_C & V_R & \\ & 0 & V_R^\dagger & H_R & -t_R \\ & & & -t_R & \ddots \end{pmatrix}.$$

The dots to the left of H_L are for the semi-infinite periodic left lead, and it is approximated by a tight-binding scheme[2] with each "site" being a block containing three layers of gold in this case (refer to the blue boxes in Figure S2), and the hopping between sites is the t_L matrix. H_L and t_L are of the size $N_L \times N_L$ with N_L the number of basis functions in a block. Similar arguments apply to the right semi-infinite lead and we introduce N_R in a similar fashion.

The self-energy due to the left lead can be written as[10,12]:

$$\Sigma_L = V_L^\dagger G_L^{surf} V_L$$

G_L^{surf} is the surface Green's function of the left lead, and is of the size $N_L \times N_L$. V_L is of the size $N_L \times N_C$. As a result, Σ_L is of the size $N_C \times N_C$.

Now we argue that, for the $N_C \times N_C$ matrix Σ_L, only the upper left $N_L \times N_L$ block should be non-zero. In the Hamiltonian and Figure S2, we allow sufficient screening in the extended molecule (hence the reason of using four layers of gold atoms in the central region), the coupling of left lead and the central region should be limited to the leftmost N_L element of the extended molecule. In other words, only the leftmost $N_L \times N_L$ block of V_L is non-zero. This is consistent with the tight-binding treatment of the semi-infinite lead (i.e., t_L is of dimension N_L). Because Γ_L is imaginary part of Σ_L, the $N_C \times N_C$ matrix Γ_L is only non-zero at the upper left $N_L \times N_L$ corner.

We use a similar block-zero form for Γ_R with only right bottom $N_R \times N_R$ block being non-zero. Those coupling matrices are calculated at PBE level. We use this form in Landauer formula to compute T(E). In Landauer formula, G is of dimension $N_C \times N_C$. Because of the block-zero form of Γ_L and Γ_R, only the upper right $N_L \times N_R$ corner of G matrix contributes to T(E).

This form is essential for eliminating numerical noise in the final T(E) result. Suppose the right bottom corner of Γ_L is not exactly zero, but its elements are at the magnitude of $\sim 10^{-7}$, then it will result in additional contributions to T(E) in Landauer formula. If the dimension of central region is $\sim 10^3$, then the additional contribution is $\sim 10^{-4}$ and is usually negligible for systems with $T(E) > 10^{-3} G_0$, but is very important for regions and systems where $T(E) < 10^{-4}$ such as the metal-porphyrins in this work.

We also note in passing that in our DFT+Σ approach, we actually modify the H_{mol} block in H_C, where:

$$H_C = \begin{pmatrix} H_l & V_l & V_{lr} \\ V_l^\dagger & H_{mol} & V_r \\ V_{lr}^\dagger & V_r^\dagger & H_r \end{pmatrix}$$

We shift the eigenvalues according to the procedure discussed in the main text and then "undiagonalize" it, i.e., H_{mol}=>$SCEC^{-1}$, where S is the overlap matrix, and column vectors of C are eigenvectors of Hmol. E = diag($\varepsilon_i + \Delta_i$), a diagonal matrix with ε_i the eigenvalues of H_{mol} and Δ_i the shift calculated from DFT+Σ in the main text. This modification of H_{mol} is done at every k-parallel point.

Experiment

1) Materials and general methods:

Chemicals were purchased from Sigma-Aldrich and used as received, unless otherwise noted. All reactions were performed in oven-dried round bottom flasks, unless otherwise noted. The flasks were fitted with rubber septa and reactions were conducted under a positive pressure of argon, unless otherwise noted. Anhydrous solvents were obtained from a Schlenk manifold with purification columns packed with activated alumina and supported copper catalyst (Glass Contour, Irvine, CA). Stainless steel syringes or cannulae were used to transfer air- and moisture-sensitive liquids. Flash column chromatography was performed employing 32-63 μm silica gel (Dynamic Adsorbents Inc). Thin- layer chromatography (TLC) was performed on silica gel 60 F_{254} plates (EMD). ^{1}H and ^{13}C nuclear magnetic resonance spectra were recorded at 300 K (unless otherwise noted) on *Bruker* DRX300 (300MHz) or *Bruker* DRX400 (400MHz) FT NMR spectrometers. High-resolution mass spectra were recorded on a *JMS-HX110 HF* mass spectrometer (ionization mode: FAB+). Uv-vis absorption spectra were taken on a Shimadzu UV-1800 spectrophotometer.

2) UV-Vis spectrum

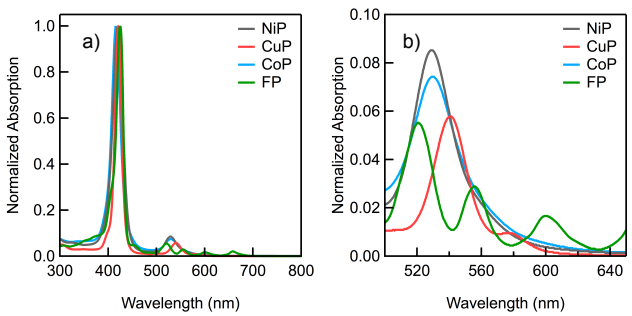

Figure S3: a) UV-vis spectrum of all porphyrins considered in this work, highlighting the B-band for all compounds. b) Q-band region of the UV-vis spectrum.

3) Synthetic procedures

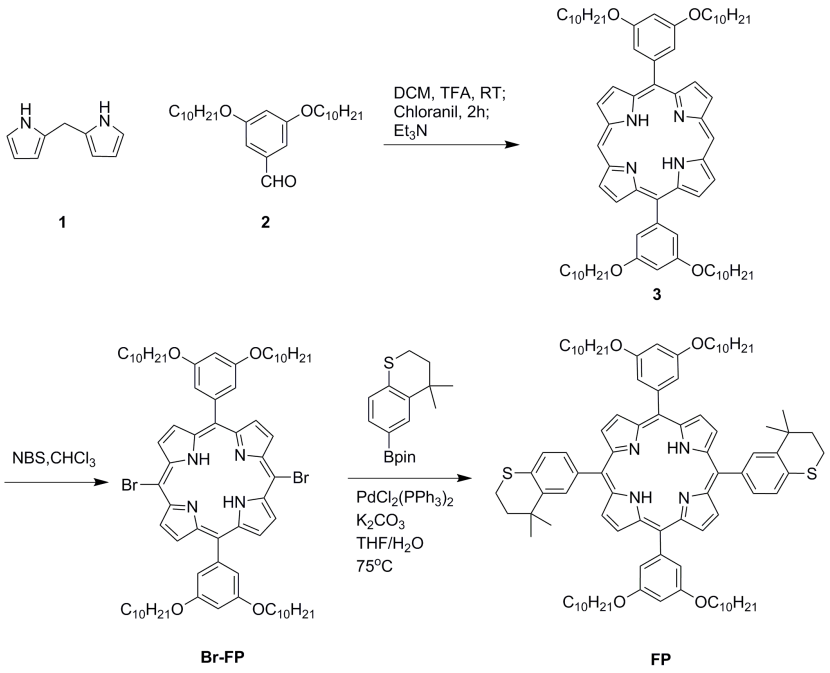

Scheme S1: Synthetic procedures for FP molecule.

1: Synthesized by following the literature procedure: *Nature Chemistry*, **2010**, *2*, 503-508.

2: Synthesized by following the literature procedure: *J. Am. Chem. Soc*, **2006**, *128*, 16083-16091.

3: To a mixture solution of **2**(11.44 g, 27.3 mmol) and **1**(4.0 g, 27.3 mmol) in CH_2Cl_2 (1.5 L) and TFA(1 mL, 13.1 mmol) was added and stirred for 12 h at 25°C. Then, p-chloranil(10.1 g, 40.95 mmol) was added and the reaction mixture was further stirred for 4 h. The reaction mixture was concentrated to a volume of 300 mL and then flash chromatographed in silica gel with CH_2Cl_2. The reaction mixture was purified by column chromatography with 70% hexane/CH_2Cl_2 and evaporated to dryness to give **3**, a reddish purple solid (6.4 g, 43%)

^{1}H NMR (400MHz, $CDCl_3$, ppm): δ 10.30(s, 2H), 9.38-9.37(d, *J* = 4.4Hz, 4H), 9.20-9.18(d, *J* = 4.4Hz, 4H), 7.43(s, 4H), 6.91(s, 2H), 4.17-4.14(t, *J* = 6.4Hz, 8H) 1.91-1.87(t, *J* = 7.2Hz, 8H), 1.55-1.48(m, 8H), 1.38-1.26(m, 48H), 0.87-0.84(t, *J* = 6.4Hz, 12H), -3.15(s, 2H).

Br-FP : *N*-bromosuccinimide (NBS; 2.15 g, 12.1 mmol) was added to a solution of **3** (6.4 g, 5.9 mmol) in $CHCl_3$ (400 mL) at 0°C and then stirred for 7 h at 25°C. The reaction mixture was quenched with acetone (20mL) and evaporated. The reaction mixture was purified by column chromatography with 50% hexane/CH_2Cl_2, where the first fraction was collected and evaporated to dryness. The residue was recrystallized from CH_2Cl_2/hexane to give **Br-FP**, a purple solid (5.4 g, 74%)

^{1}H NMR (400MHz, $CDCl_3$, ppm): δ 9.60-9.59 (d, J = 4.8Hz, 4H), 8.96-9.95(d, J = 4.8Hz, 4H), 7.32(s 4H), 6.90(s, 2H), 4.14-4.11(t, J = 6.4Hz, 8H), 1.91-1.84(m, 8H), 1.54-1.51(m, 8H), 1.35-1.17(m, 48H), 0.86(t, J = 6.4Hz, 12H), -2.74(s, 2H).

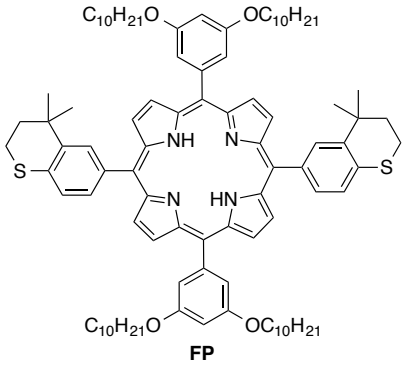

FP

Scheme S2: Structure of FP molecule.

FP: **Br-FP**(600mg, 0.5mmol), thiochroman pinacol ester (440mg, 1.4mmol), $Pd(PPh_3)_2Cl_2$ (20mg, 0.025mmol) and K_2CO_3 (200mg, 1.4mmol) were charged in a 100mL 2-neck round bottom flask with a condenser under argon, and then 50mL of degassed THF/H_2O (4/1) was added via a syringe. The reaction was heated at 70^{o}C overnight under dark and then cooled down to room temperature. Water (50mL) was added, the resulting blue solution was extracted with DCM (50mL x 3). The combined organic solvents were washed with brine and dried over Mg_2SO_4. After removing solvents, the residue was purified by flash chromatography (hexane/dichloromethane=3/2) to give a blue solid (450mg, 65%).

^{1}H NMR (400MHz, $CDCl_3$, ppm): δ 8.96(d, *J* = 4.8Hz, 4H), 8.88(d, *J* = 4.8Hz, 4H), 8.21 (s, 2H), 7.88(t, *J* = 7.2Hz, 2H), 7.46(d, *J* = 8.0Hz, 2H), 7.37(s, 4H), 6.88(t, *J* = 2.4Hz, 2H), 4.11(t, *J* = 6.4Hz, 8H), 3.28-3.25(m, 4H), 2.23-2.20(m, 4H), 1.87-1.84(m, 8H), 1.54-1.50(m, 20H), 1.35-1.17(m, 48H), 0.84(t, *J* = 6.8Hz, 12H).

HR-MS (FAB) *m/z* calcd for $C_{94}H_{126}N_4O_4S_2$: 1440.19, found: 1440.30.

Uv-Vis (CH_2Cl_2): 425nm, Q bands(521nm, 556nm, 600nm, 658nm).

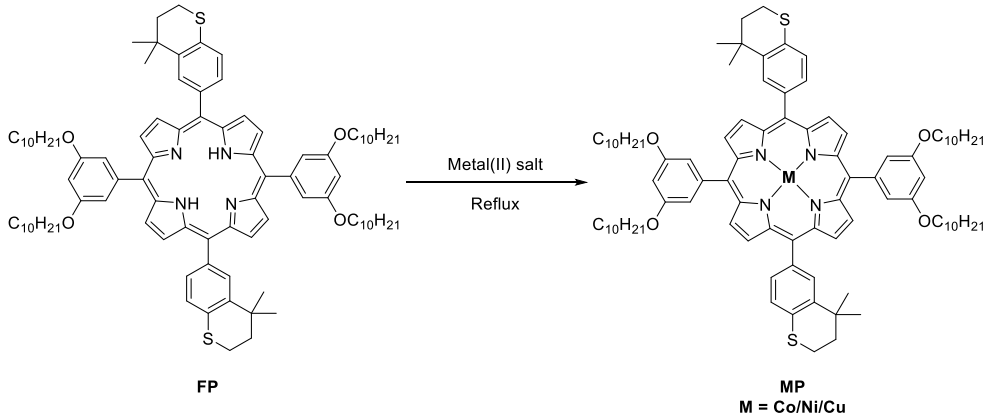

Scheme S3: Synthesis of MP (M=Co/Ni/Cu) molecules from FP molecule.

MP: insertion of different metal cations into the **FP** porphyrin core was carried out by following literature procedures[13, 14, 15].

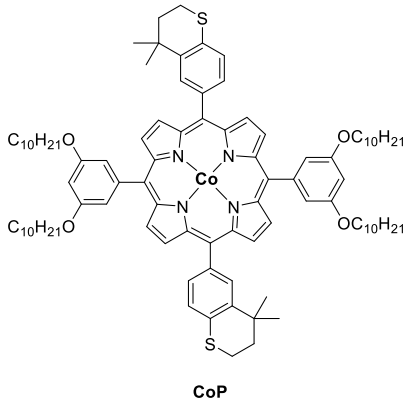

Scheme S4: Structure of CoP molecule.

CoP: 60mg of **FP** and 200 mg Co(II) Diacetylcarbonate were refluxed overnight in 8mLTHF. The completion of the reaction was monitored by TLC. After cooled down to room temperature, the solution was partitioned between 40mL $CHCl_3$ and 20mL H_2O. The organic layer was further washed with H_2O and brine, dried over Na_2SO_4. After removal of solvents, the residue was purified by preparative TLC (hexane/dichloromethane=1/1, with 5% v/v Et_3N) to give **CoP**. The yield was >90%.

Uv-Vis (CH_2Cl_2): 415nm, Q bands(529nm, 565nm).

HR-MS (FAB) *m/z* calcd for $C_{94}H_{124}N_4O_4S_2Co$: 1497.10, found: 1497.20.

NiP, CuP:

60mg of **FP** was first dissolved in 5mL $CHCl_3$. To the above solution, 5mL saturated methanol solution of $Ni(OAc)_2$ or $Cu(OAc)_2$ or $Zn(OAc)_2$ was added. The mixture was further refluxed overnight in dark. The completion of the reaction was monitored by TLC. After cooled down to room temperature, the solution was partitioned between 30mL $CHCl_3$ and 30mL H_2O. The organic layer was further washed with H_2O and brine, dried over Na_2SO_4. After removal of solvent, the residue was purified by preparative TLC (hexane/dichloromethane=3/2, with 5% v/v Et_3N). The yield was >90%.

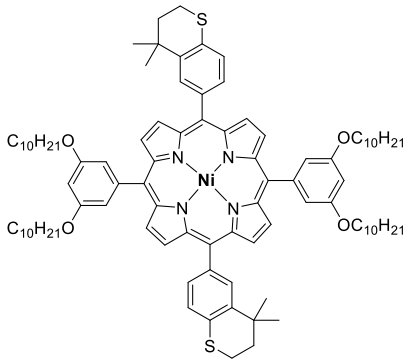

NiP

Scheme S5: Structure of NiP molecule.

NiP: ^1H NMR (400MHz, $CDCl_3$, ppm): δ 8.87(d, *J* = 6.4Hz, 4H), 8.80(d, *J* = 6.4Hz, 4H), 8.11(s, 2H), 7.80(s, 2H), 7.19(d, *J* = 2.8Hz, 4H), 6.82(d, *J* = 2.8Hz, 2H), 4.08(t, *J* = 8.4Hz, 8H), 2.20(m, 4H), 1.87-1.80(m, 8H), 1.52-1.10(m, 68H), 0.87(t, *J* = 6.8Hz, 12H).

HR-MS (FAB) *m/z* calcd for $C_{94}H_{124}N_4O_4S_2Ni$: 1496.86, found: 1496.39.

Uv-Vis (CH_2Cl_2): 421nm, Q bands(529nm, 560nm).

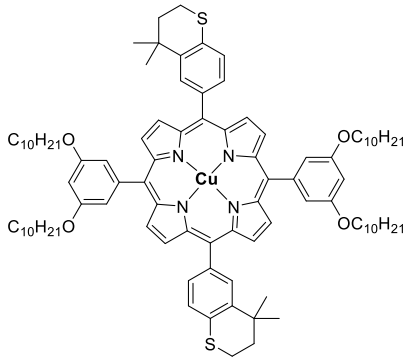

CuP

Scheme S6: Structure of CuP molecule.

CuP: Uv-Vis (CH_2Cl_2): 421nm, Q bands(541nm, 579nm)

HR-MS (FAB) *m/z* calcd for $C_{94}H_{124}N_4O_4S_2Cu$: 1501.72, found: 1501.21.

References:

1) Quek, S. Y.; Venkataraman, L.; Choi, H. J.; Louie, S. G.; Hybertsen, M. S.; Neaton, J. B. *Nano Lett.* 2007, 7, 3477-3482.

2) Neaton, J. B.; Hybertsen, M. S.; Louie, S. G. *Phys. Rev. Lett.* 2006, 97, 216405.

3) Stein, T.; Eisenberg, H.; Kronik, L.; Baer, R. *Phys. Rev. Lett.* 2010, 105, 266802.

4) Refaely-Abramson, S.; Sharifzadeh, S.; Govind, N.; Autschbach, J.; Neaton, J. B.; Baer, R.; Kronik, L. *Phys. Rev. Lett.* 2012, 109, 226405.

5) Refaely-Abramson, S.; Sharifzadeh, S.; Jain, M.; Baer, R.; Neaton, J. B.; Kronik, L. *Phys. Rev. B* 2013, 88, 081204.

6) Khandelwal, S. C.; Roebber, J. L. *Chem. Phys. Lett.* 1975, 34, 355–359.

7) Paulsson, M.; Brandbyge, M. *Phys. Rev. B* 2007, 76, 115117.

8) Landauer, R. *IBM J. Res. Dev.* 1957, 1, 223–231.

9) Meir, Y.; Wingreen, N. S. *Phys. Rev. Lett.* 1992, 68, 2512–2515.

10) Brandbyge, Mads; Mozos, José-Luis; Ordejón, Pablo; Taylor, Jeremy; Stokbro, Kurt, *Phys. Rev. B* 2002, 65, 165401

11) Choi, H. J.; Cohen, M. L.; Louie, S. G. *Phys. Rev. B* 2007, 76, 155420.

12) Taylor, Jeremy; Guo, Hong; Wang, Jian, *Phys. Rev. B* 2001, 63, 245407.

13) Mori, Shigeki; Ishii, Kazuyuki; Hirakawa, Yuichiro; Nakamura, Ryuhei; Hashimoto, Kazuhito, *Inorg. Chem.*, 2011, 50, 2037-2039.

14) Fu, Shitao; Zhu, Xunjin; Zhou, Guijiang; Wong, Wai-Yeung; Ye, Cheng; Wong, Wai-Kwok; Li, Zaoying, *Eur. J. Inorg. Chem.*, 2007, 2004-2013.

15) Fukuzumi, Shunichi; Ohkubo, Kei; Zhu, Weihua; Sintic, Maxine; Khoury, Tony; Sintic, Paul J.; E, Wenbo; Ou, Zhongping; Crossley, Maxwell J.; Kadish, Karl M. *J. Am. Chem. Soc.*, 2008, 130(29), 9451-9458.

NMR Spectra

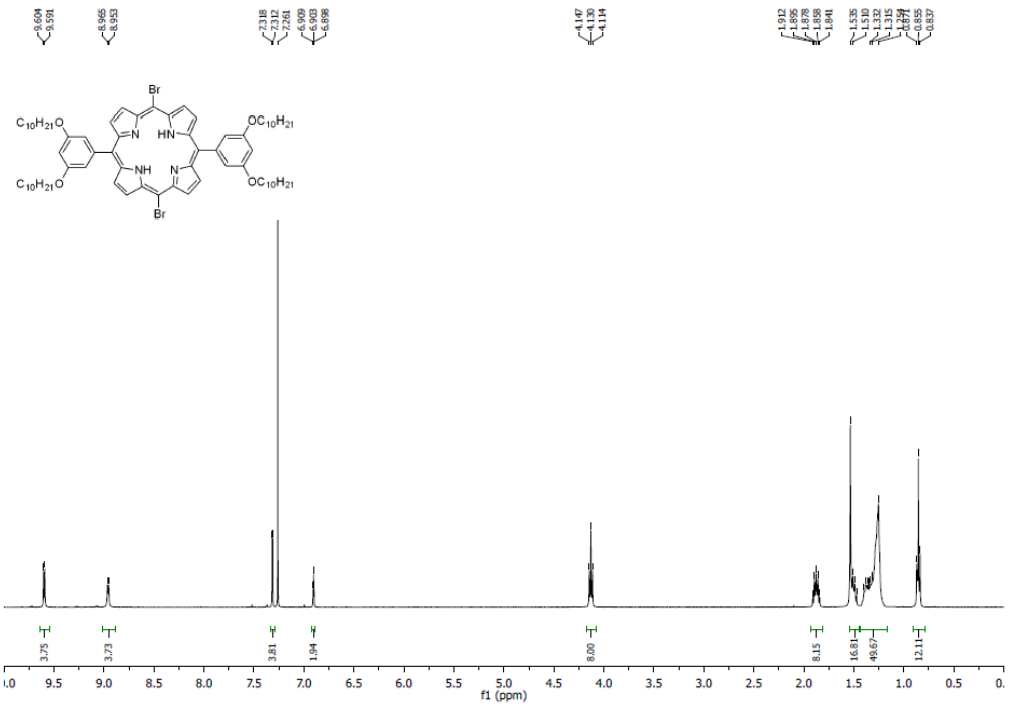

Scheme S7: NMR spectrum for Br-FP molecule.

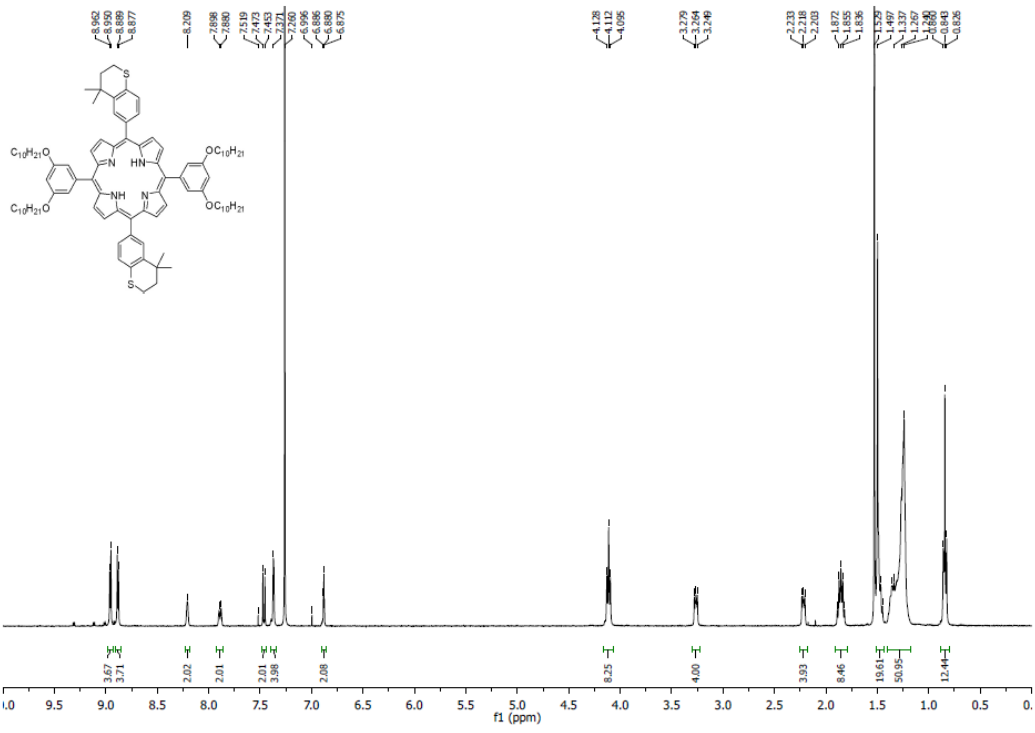

Scheme S8: NMR spectrum for FP molecule.

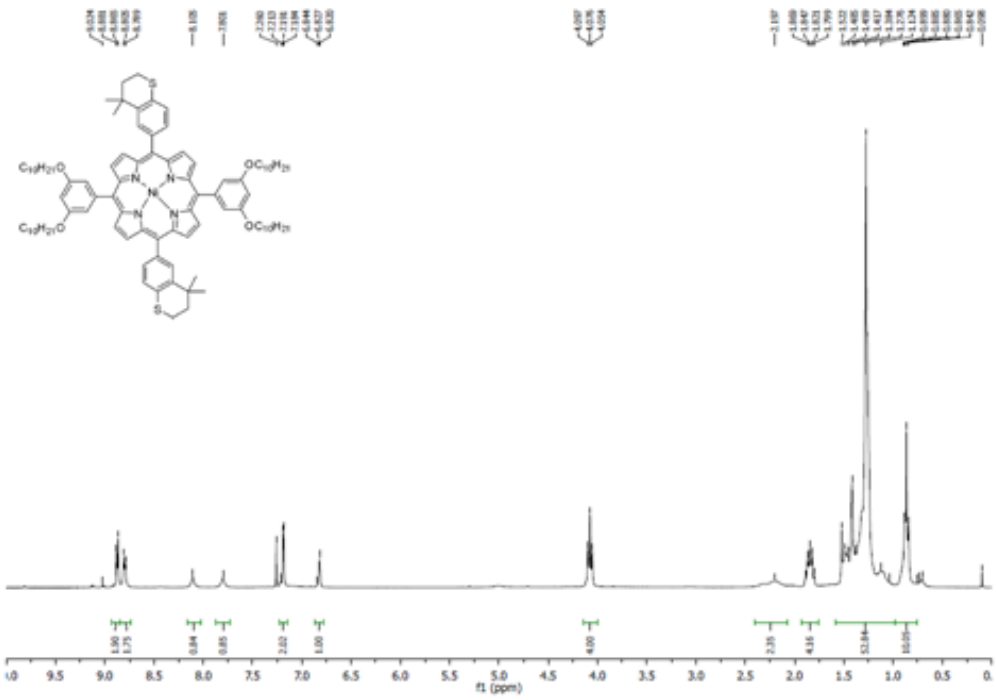

Scheme S9: NMR spectrum for NiP molecule.